Competitive C–H and O–D bond fission channels in the UV photodissociation of the deuterated hydroxymethyl radical CH_2OD

Lin Feng, Andrey V. Demyanenko, and Hanna Reisler
Department of Chemistry, University of Southern California, Los Angeles, California 90089-0482

(Received 5 December 2003; accepted 13 January 2004)

Photodissociation studies of the CH_2OD radical in the region 28 000–41 000 cm^{-1} (357–244 nm), which includes excitation to the $3s$, $3p_x$, and $3p_z$ states, are reported. H and D photofragments are monitored by using resonance-enhanced multiphoton ionization (REMPI) from the onset of H formation at ~30 500 cm^{-1} to the origin band region of the $3p_z(^2A'')\leftarrow 1\,^2A''$ transition at 41 050 cm^{-1}. Kinetic energy distributions $P(E_T)$ and recoil anisotropy parameters as a function of kinetic energy, $\beta_{\text{eff}}(E_T)$, are determined by the core sampling technique for the channels producing H and D fragments. Two dissociation channels are identified: (I) $D+CH_2O$ and (II) $H+CHOD$. The contribution of channel II increases monotonically as the excitation energy is increased. Based on the calculations of Hoffmann and Yarkony [J. Chem. Phys. **116**, 8300 (2002)], it is concluded that conical intersections between $3s$ and the ground state determine the final branching ratio even when initial excitation accesses the $3p_x$ and $3p_z$ states. The different β_{eff} values obtained for channels I and II (−0.7 and ~0.0, respectively) are attributed to the different extents of out-of-plane nuclear motions in the specific couplings between $3s$ and the ground state (of A' and A'' symmetry, respectively) that lead to each channel. The upper limit to the dissociation energy of the C–H bond, determined from $P(E_T)$, is $D_0(\text{C–H})=3.4\pm0.1$ eV (79 ± 2 kcal/mol). Combining this value with the known heats of formation of H and CH_2OD, the heat of formation of CHOD is estimated at $\Delta H_f^0(\text{CHOD})=24\pm2$ kcal/mol. © *2004 American Institute of Physics.*
[DOI: 10.1063/1.1665880]

I. INTRODUCTION

The hydroxymethyl radical (CH_2OH) and its isomer, the methoxy radical (CH_3O), have long been recognized as important intermediates in hydrocarbon combustion and in atmospheric processes. They are significant products in the reaction of $O(^1D)$ with methane and ethane,[1,2] and reactions of Cl atoms and OH radicals with methanol yield predominantly CH_2OH.[3–5] According to *ab initio* calculations, the lowest excited electronic states of CH_2OH have a predominant Rydberg character—specifically, the $3s$, $3p_x$, $3p_y$, and $3p_z$ states.[6,7] Of these four states, only $3p_y$ does not carry oscillator strength. Electronic spectra of the hydroxymethyl radical to these states have been measured by ultraviolet (UV) absorption,[3,8] resonance-enhanced multiphoton ionization (REMPI),[4,9–11] depletion, and photofragment yield spectroscopies.[11,12] The transitions to the $3p_x$ and $3p_z$ states exhibit distinct vibrational structures, while the transition to the $3s$ state is broad and structureless.

Recent photodissociation dynamics studies of the deuterated hydroxymethyl radical CH_2OD have helped in characterizing the potential energy surfaces (PESs) participating in the dissociation. $D+CH_2O$ was identified as a major channel following 365–318 nm excitation to the $3s$ state and ~244 nm excitation to the origin band of the $3p_z$ state.[12–14] Isomerization to the methoxy radical was not observed.

A theoretical study of the conical intersections involved in the dissociation has been recently reported by Hoffman and Yorkony (HY).[15] In this calculation, conical intersections connecting the $3p_x$ and $3s$ states and the $3s$ and ground states have been found both along the C–H and O–H coordinates. These intersections promote efficient nonadiabatic transitions and are important in understanding the dissociation mechanism.

In this report, photodissociation studies of CH_2OD in the region 28 000–41 000 cm^{-1} (357–244 nm) are described. This region includes, in addition to the transition to the $3s$ state, the origin bands of the transitions to the $3p_x$ and $3p_z$ states.[11] H and D photofragments are monitored from the onset of H formation (at ~30 500) up to 41 000 cm^{-1}. Combining the experimental findings with conical intersection calculations and thermochemical data, we propose that the most likely channels responsible for H and D formation are

$$\text{(I)}\quad CH_2OD\rightarrow CH_2O+D,\quad \Delta H=1.32\pm0.07\ \text{eV},$$

$$\text{(II)}\quad CH_2OD\rightarrow HCOD+H,\quad \Delta H=3.4\pm0.1\ \text{eV}.$$

Kinetic energy distributions, $P(E_T)$, and recoil anisotropy parameters as a function of kinetic energy release, $\beta_{\text{eff}}(E_T)$, are reported for each channel at selected excitation energies. These data demonstrate fundamental differences in the dissociation dynamics into these two channels and provide further insight into the dissociation mechanism. It is concluded that the conical intersections between $3s$ and the ground state determine the final branching ratio, even when initial excitation is to the $3p_x$ or $3p_z$ state. In other words, sequential conical intersections terminating in the ground electronic state lead eventually to C–H and O–D bond fission channels.

In addition, the $P(E_T)$ measurements enable the first determination of the C–H bond dissociation energy of CH_2OD. This, in turn, leads to an experimental estimation of the heat of formation of CHOD, a value that can be compared with theoretical calculations.

II. EXPERIMENT

The experimental apparatus and procedures have been described in detail elsewhere.[11,12] A mixture of 4% CH_3OD or CH_3OH (Aldrich, used without further purification) and ~1% Cl_2 (Air gas, 99.5%) in He at 2 atm total pressure is prepared in a 4-liter glass bulb. A piezoelectrically driven pulsed nozzle operating at 10 Hz introduces this mixture to the source region of a differentially pumped vacuum chamber. A 355-nm laser pulse beam (Spectra Physics, GCR-11; 8 mJ, focused by a 30-cm-f.l. cylindrical lens) crosses the edge of a 1-mm-diam quartz tube attached in front of the nozzle orifice. The 355 nm radiation dissociates Cl_2, and the Cl atoms react rapidly with $CH_3OD(CH_3OH)$, creating $CH_2OD(CH_2OH)$.

The radicals generated in the collisional part undergo cooling during the supersonic expansion. The $CH_2OD(H)$ radicals pass through a 1.51-mm-diam skimmer (Beam Dynamics) and reach the photodissociation region vibrationally cold. A ~10 K rotational temperature is estimated from the $1+1'$ two-color REMPI spectrum obtained via the $3p_z$ state.[9] The radicals are intersected by the UV pump laser beam. The UV radiation is obtained from a seeded Nd:YAG laser-pumped OPO&OPA (Continuum, PL8000/Sunlite/FX-1; 0.5 mJ, 40-cm-f.l. lens) system. The H and D photofragments are probed by $1+1'$ two-color REMPI via the $L-\alpha$ transition at 121.6 nm. To generate 121.6 nm radiation, the doubled output (~365 nm, ~2 mJ) of a Nd:YAG pumped dye laser system (Continuum, PL8010/ND6000, LDS 751) is focused into a mixture of Kr:Ar (120:490 Torr) in a tripling cell. A MgF_2 lens (75-mm-f.l. lens) then refocuses the tripled 121.6 nm radiation into the chamber. The pump and probe laser beams are counterpropagating and cross the molecular beam at a right angle. The time delay between the pump and probe laser beams is kept at 0–2 ns.

Time-of-flight (TOF) distributions of the photofragments are recorded by the core-sampling technique combined with REMPI detection of the products. This method has been described in detail elsewhere.[12,13,16] In brief, the core-sampling arrangement consists of a two-stage ion acceleration region, an 18-cm field-free drift region, and a 4-mm-diam aperture installed in front of a multichannel plate detector (MCP, Galileo, 25 mm). The ion detector is positioned parallel to the plane defined by the molecular and laser beams. The aperture is mounted on a linear motion feedthrough (MDC, BLM-133-4) to allow alternation between total ion collection and core sampling. The core sampling technique utilizes a spatial restriction in the ion detection in order to eliminate contributions from off-axis ions, thereby yielding the speed distribution of the recoiling fragments in a straightforward manner. In this method, TOF distributions of the photofragements are recorded with parallel and perpendicular polarization of the photolysis laser: therefore, both $P(E_T)$ and $\beta_{\text{eff}}(E_T)$ of the photofragments are obtained.

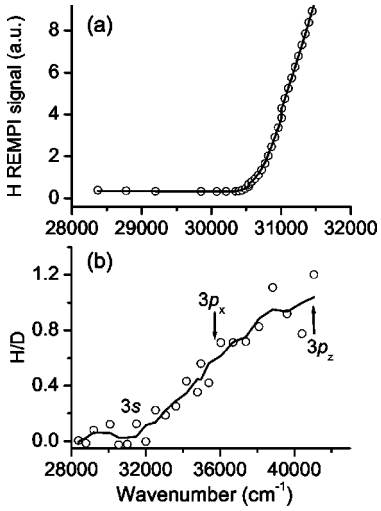

FIG. 1. (a) H fragment REMPI signal and (b) H/D ratio dependence on CH_2OD excitation energy. Open circles are data points; solid lines are guides to the eye.

III. RESULTS

Photofragment yield spectra of D products from CH_2OD following excitation to the $3s$, $3p_x$, and $3p_z$ states have been reported before at energies above the threshold of D formation at 26 000 cm^{-1}.[11] The H product signal observed in our experiment, on the other hand, starts to appear only at 30 540±1000 cm^{-1}—i.e., 4540 cm^{-1} higher than the onset of D production. The difference in thresholds suggests that the H and D channels are produced by different pathways. As shown in Fig. 1(a), the H signal rises sharply above its threshold. In Fig. 1(b), the H/D ratio is plotted versus excitation energy in the region 28 000–41 000 cm^{-1} (357–244 nm), which encompasses absorption to the $3s$, $3p_x$, and $3p_z$ states. The ratio increases smoothly with excitation energy, exhibiting no sharp changes when the band origins of the transitions to the $3p_x$ and $3p_z$ states are traversed. Considering the broadness of the $3s(^2A')\leftarrow 1\,^2A''$ and the $3p_x(^2A')\leftarrow 1\,^2A''$ absorption spectra,[11] the scan step sizes used in obtaining the curves shown in Fig. 1 are sufficient. In order to better understand the dissociation mechanisms responsible for H and D production, detailed studies have been carried out near the band origins of the transitions to the $3p_x$ and $3p_z$ states.

A. Excitation to the $3p_z(2\,^2A'')\leftarrow 1\,^2A''$ origin band

Figure 2(a) displays the $1+1'$ REMPI spectrum of jet-cooled CH_2OD in the origin band region of the $3p_z(2\,^2A'')\leftarrow 1\,^2A''$ transition. Figure 2(b) shows the corresponding H photofragment yield spectrum—namely, the variation of the H atom signal obtained as the excitation laser is scanned through the band origin region while the probe laser wavelength is fixed at the H atom detection wavelength. The similarity of the CH_2OD^+ and H^+ bands demonstrates that H is a product of CH_2OD photodissociation. Due to a large H background, the H product was not discernible in our previous experiments.[12]

In order to check the isotopic purity of the CH_2OD sample, REMPI spectra in the region of the $3p_z$ origin band

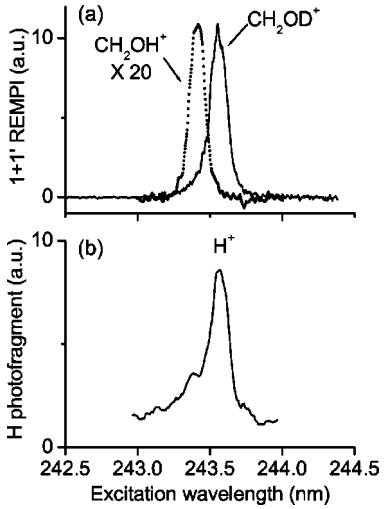

FIG. 2. (a) $1+1'$ REMPI spectra of CH_2OD (solid line) and CH_2OH (dotted line) in the origin band region of the $3p_z(2\,^2A'')\leftarrow 1\,^2A''$ transition. (b) The H photofragment yield spectrum obtained in CH_2OD dissociation.

were obtained by monitoring both mass 32 and 31 (CH_2OD^+ and CH_2OH^+, respectively). From the signals shown in Fig. 2(a), we estimate that ~5% CH_2OH isotopic contamination is present (assuming that the absorption cross sections of CH_2OD and CH_2OH are the same). The source of CH_2OH is possibly CH_3OH contamination in the CH_3OD precursor. Because the peak positions of the REMPI signals of CH_2OD and CH_2OH are well separated in energy [see Fig. 2(a)], the products obtained with 243.6 nm excitation originate only from CH_2OD and are not affected by CH_2OH contamination.

The c.m. translational energy distribution $P(E_T)$ and $\beta_{\text{eff}}(E_T)$ of the H channel obtained with 243.6 nm excitation are shown in Figs. 3(a) and 3(b), respectively. For comparison, the c.m. $P(E_T)$ of the D channel at the same wavelength is also shown [Fig. 3(c)]. The maximum c.m. translational energy release in the D channel is the same as that reported before by Conroy *et al.*[12] and is consistent with the maximum value of 3.76 eV obtained by using $D_0(\text{O–D}) = 1.32$ eV.

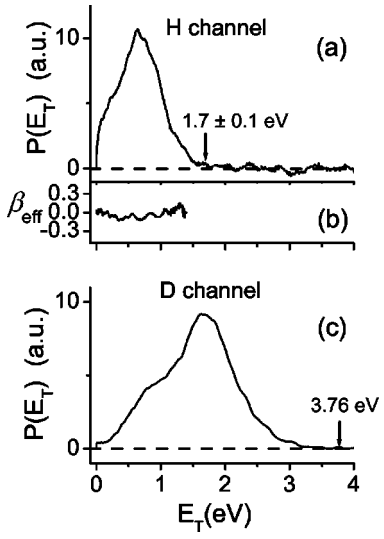

FIG. 3. (a) The c.m. E_T distribution and (b) E_T-dependent β_{eff} distribution of the H channel. (c) The c.m. E_T distribution of the D channel. The distributions are obtained with 243.6 nm photolysis of CH_2OD—(the peak in the origin band of the $3p_z(2\,^2A'')\leftarrow 1\,^2A''$ transition). The arrow in panel (a) indicates the maximum c.m. E_T release in the H channel. In (c), the arrow marks the value of $E_T^{\max}$ for $CH_2OD\rightarrow CH_2O(^1A_1)+D$ calculated using $D_0(\text{O–D}) = 1.32$ eV.

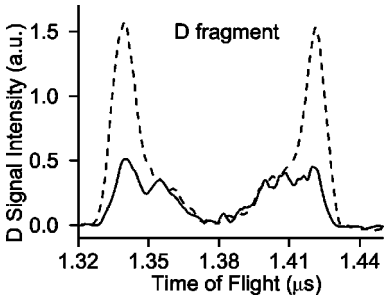

FIG. 4. Core-sampling TOF spectra of D photofragments from CH_2OD following excitation to the $3p_x$ state at 285.5 nm. Signals from parallel (solid line) and perpendicular (dashed line) polarization of the photolysis laser beam are shown after background subtraction and normalization to laser power.

The c.m. $P(E_T)$ corresponding to the H channel is much narrower than that of D and has a maximum value $E_T^{\max} = 1.7 \pm 0.1$ eV. The H product most likely derives from channel II—i.e., C–H bond fission. The C–H bond dissociation energy $D_0(\text{C–H}) = 3.4 \pm 0.1$ eV is obtained by energy conservation: $E_{h\nu}(243.6\,\text{nm}) = D_0(\text{C–H}) + E_T^{\max} - E_{\text{int}}$, where E_{int} is the internal energy of the parent hydroxymethyl radical, which is negligible in the cold beam expansion.

B. Excitation to the $3p_x(^2A')\leftarrow 1\,^2A''$ origin band

D and H products are also observed following excitation to the origin band of the $3p_x(^2A')\leftarrow 1\,^2A''$ transition at 285.5 nm (35 026 cm^{-1}). Figure 4 shows D-atom core-sampled TOF profiles obtained with parallel (solid line) and perpendicular (dashed line) polarization of the photolysis laser beam. The spectra shown are obtained after subtracting background signals taken by blocking the 355-nm laser beam. In Fig. 5, the corresponding $P(E_T)$ and $\beta_{\text{eff}}(E_T)$ of the D product are presented. The transformation from TOF spectra to E_T distributions has been described before.[12]

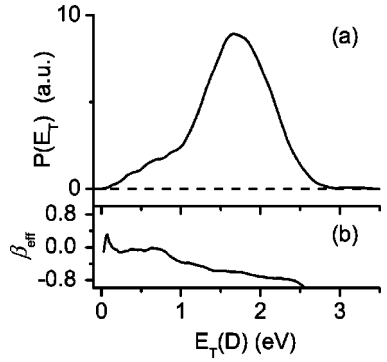

FIG. 5. (a) D photofragment translational energy distribution and (b) the corresponding E_T-dependent β_{eff} distribution. The distributions are obtained following excitation to the origin band of the $3p_x(^2A')\leftarrow 1\,^2A''$ transition at 285.5 nm.

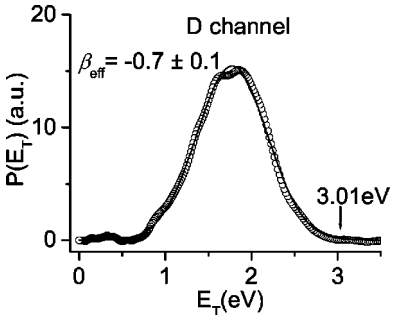

FIG. 6. The c.m. E_T distribution (open circles) of channel I obtained following excitation to the origin band of the $3p_x(^2A')\leftarrow 1\,^2A''$ transition at 285.5 nm. The solid line shows a Gaussian fitting to the data. The arrow indicates the $E_T^{\max}$ value calculated using $D_0(\mathrm{O–D})=1.32$ eV.

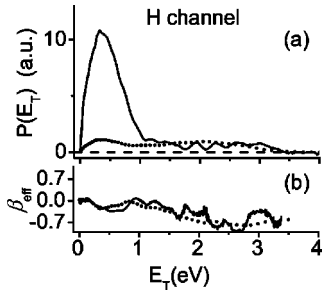

FIG. 7. (a) The c.m. E_T distribution and (b) the E_T-dependent β_{eff} distribution of the H channel from photolysis at 285.5 nm. The solid and dotted lines represent the corresponding values obtained by using CH_3OD and CH_3OH as precursors, respectively.

The D photofragment E_T distribution exhibits two features with markedly different β_{eff} values. The high-energy component that extends to ~3 eV has an almost constant β_{eff} of -0.7 ± 0.1, while the low-energy peak at ~1 eV is isotropic ($\beta_{\mathrm{eff}}\approx 0$). The change in $\beta_{\mathrm{eff}}(E_T)$ suggests that two sources contribute to the D signal. A similar change in $\beta_{\mathrm{eff}}(E_T)$ was observed in the study of the D product obtained via excitation to the $3s$ state.[13] In that study, the dependence of the TOF spectra on experimental conditions was investigated in a controlled way by varying the position of the Cl_2 photolysis laser beam along the quartz tube and the $[Cl_2]/[CH_3OD]$ ratio. Based on the variation of the low-kinetic-energy D component with experimental conditions and its small intensity under conditions that disfavor secondary reactions, it was concluded that the signal associated with $\beta_{\mathrm{eff}}=0$ at low E_T derived from secondary reactions. The isotropic part observed in the present study appears to be similar and therefore can be removed by the same procedure.[13] By assuming a constant value of $\beta_{\mathrm{eff}}\approx 0$ for the slow component and $\beta_{\mathrm{eff}}=-0.7$ for the fast one, the relative contributions $P_i(E_T)$ ($i=$I or II) of the two sources can be deconvoluted using the equations $P(E_T)=P_{\mathrm{I}}(E_T)+P_{\mathrm{II}}(E_T)$ and $\beta_{\mathrm{eff}}(E_T)=\chi_{\mathrm{I}}(E_T)\beta_{\mathrm{eff\,I}}+\chi_{\mathrm{II}}(E_T)\beta_{\mathrm{eff\,II}}$, where $\chi_i(E_T)=P_i(E_T)/P(E_T)$.

The c.m. $P(E_T)$ resulting only from the CH_2OD precursor is shown in Fig. 6. It is well described by a Gaussian function, with a peak at $E_T^{\mathrm{peak}}=1.77$ eV and width $\Delta E_T=0.83$ eV [full width at half maximum (FWHM)]. The arrow in Fig. 6 indicates the maximum allowed c.m. translational energy of the products, $E_T^{\max}=3.01$ eV, calculated using $D_0=1.32$ eV for the $CH_2OD\rightarrow CH_2O(^1A_1)+D$ channel. This value is in good agreement with the observed value. This confirms that O–D bond breaking is responsible for the D product at this energy. The negative β_{eff} value of -0.7 ± 0.1 is consistent with the $3p_x(^2A')\leftarrow 1\,^2A''$ transition dipole moment $\boldsymbol{\mu}$ being perpendicular to the plane of $CH_2OD(3p_x)$. It also suggests that the dissociation from the $3p_x$ state is rapid compared to rotation about an in-plane axis.

The c.m. translational energy distribution $[P_1(E_T)]$ and $\beta_{\mathrm{eff}}(E_T)$ associated with the H product at the same wavelength is shown in Fig. 7 as solid lines. A rather long tail, extending up to 3.5 eV, is observed in $P_1(E_T)$. The tail, which corresponds to a negative β_{eff} value, is due to H products deriving from the 5% CH_2OH contaminant discussed in Sec. III A. The UV absorption bands of CH_2OH and CH_2OD to the $3p_x$ state are much broader than the corresponding bands to the $3p_z$ state, and they overlap spectrally in this region.[11] Consequently, both CH_2OH and CH_2OD dissociate following 285.5 nm excitation and contribute to the H signal.

In order to separate the H contribution from the two isotopic precursors, the c.m. translational energy distribution $P_2(E_T)$ and $\beta_{\mathrm{eff}}(E_T)$ for the H channels from CH_2OH are recorded in a separate experiment at the same wavelength and are shown in Fig. 7 as dotted lines. The $P_2(E_T)$ amplitude has been normalized to fit the tail of $P_1(E_T)$. The similarity of the maximum translational energy and the anisotropy parameters of the H channel in the tail region obtained in CH_2OD and CH_2OH photodissociation supports our conclusion that this tail arises from the small CH_2OH contamination in the molecular beam. Notice that $P_2(E_T)$ displays two distinct features. In analogy with the simultaneous C–H and O–D bond fission channels in the dissociation of CH_2OD, they are attributed to C–H and O–H bond breaking. We also note that the low-kinetic-energy part corresponding to C–H dissociation gives isotropic β_{eff}, while the high-kinetic-energy region corresponding to O–H fission gives β_{eff} close to -1, which is consistent with the β_{eff} values observed for the C–H and O–D bond fission channels of CH_2OD.

The contribution of H from CH_2OH is removed by subtracting $P_2(E_T)$ from $P_1(E_T)$. The resulting c.m. $P(E_T)$ of the H channel from pure CH_2OD is shown in Fig. 8. The maximum translational energy 1.1 ± 0.2 eV is ~1.9 eV lower

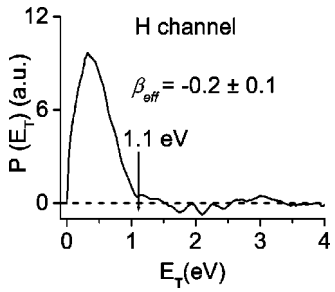

FIG. 8. The c.m. E_T distribution corresponding only to channel II following photolysis at 285.5 (see the text for details). The arrow indicates the value of $E_T^{\max}$.

than that for the D channel and corresponds to $D_0(\mathrm{C–H}) = 3.2 \pm 0.2$ eV. The larger error bar is due to the CH_2OH contaminant. Nevertheless, this value is consistent with the 3.4 ± 0.1 eV value obtained following excitation to the $3p_z$ state at 243.6 nm, confirming that direct C–H bond fission takes place. Also note that, again, the H angular distribution, which corresponds to $\beta_{\mathrm{eff}} = -0.2 \pm 0.1$, is more isotropic than that of the D channel ($\beta_{\mathrm{eff}} = -0.7$).

IV. DISCUSSION

In the electronic transitions from the ground state to the $3s$, $3p_x$, and $3p_z$ states, the radical's unpaired π^*_{CO} antibonding electron is promoted to a nonbonding Rydberg orbital. Although Rydberg states of the dissociating species correlate diabatically with Rydberg states of products, only ground-state products are observed in our experiments. Therefore, Rydberg–valence interactions and nonadiabatic surface crossings must participate in the dissociation.

A. Mechanism of dissociation from Rydberg states

The photofragment yield spectra of the D and H fragments from CH_2OD show that the onset of H production is 4540 cm^{-1} higher than that of D, indicating that two separate steps contribute to the formation of these products. The H/D ratio exhibits a monotonic increase with excitation energy, with no significant change as the radical is excited to different Rydberg states. This suggests that the dissociation mechanism following excitation to the $3s$, $3p_x$, and $3p_z$ states shares a common step.

The photodissociation dynamics from the $3p_x$ state involves conical intersections between the $3p_x$ and the $3s$ states and $3s$ and the ground state. Hoffmann and Yarkony located several conical intersection seams that provide efficient pathways for radiationless decay.[15] Following $3p_x(^2A') \leftarrow 1\,^2A''$ excitation, a low-energy portion of the $3p_x/3s$ seam of conical intersection is accessed at large C–H bond distance. From this seam, separate paths on the $3s$ PES lead to $3s$/ground-state conical intersection seams along the C–H and O–D coordinates. Finally, dissociation on the ground state yields HCOD+H and CH_2O+D products.

The lowest energy of the $3s$/ground-state intersection seam along the O–D coordinate is calculated at 2.87 eV (23 207 cm^{-1}), below the threshold of the $3s(^2A') \leftarrow 1\,^2A''$ transition. Thus CH_2OD can dissociate to CH_2O+D even in excitation to the onset of this transition, consistent with the similarity of the absorption spectrum of the $3s(^2A') \leftarrow 1\,^2A''$ transition and D photofragment yield spectrum.[11] On the other hand, the corresponding calculated energy location of the intersection along the C–H coordinate is higher, at 4.5 eV ($\sim$36 387 cm^{-1}). This is consistent with the higher threshold observed for H production than for D. The observed threshold for channel II is only 3.8 eV, lower than the value calculated by HY, but according to HY, their value may be overestimated.[15]

In the dissociation from the $3p_x$ state, the angular distribution of the products of channel II is more isotropic than that for channel I. Since the $3p_x(^2A') \leftarrow 1\,^2A''$ transition dipole moment $\boldsymbol{\mu}$ is perpendicular to the plane of CH_2OD, $\beta_{\mathrm{eff}} = -1$ is expected for fast dissociation without geometry change. According to HY, the radical reaches the $3s$ state from the $3p_x$ state via a single conical intersection. In the subsequent step, it reaches the ground state through two different conical seams. The broad spectrum of the $3p_x(^2A') \leftarrow 1\,^2A''$ transition[11] suggests that the lifetime of the $3p_x$ state is short—i.e., less than a picosecond. Therefore, we propose that the more isotropic β_{eff} value of channel II is due to out-of-plane motions required to access the intersection seams between the upper and lower states.

The $g-h$ plane defined by HY provides a graphic representation of the energy differences and couplings between two zeroth-order PESs in the vicinity of their conical intersection. This plane establishes a connection between nuclear motion and conical topography. The h vectors calculated by HY for the two intersections between $3s$ and the ground state are perpendicular to the molecular plane. This agrees with our conjecture of the importance of out-of-plane motions in enhancing the coupling matrix elements. As the $3s$ (A') and ground (A'') states are of different symmetry, the vibronic couplings that induce the interaction between them must be of A'' symmetry—e.g., out-of-plane motions. Large out-of-plane motions along the C–H crossing seam, such as CH_2 wag (of A'' symmetry), can reduce the anisotropy observed for channel II. It is noteworthy that the h vector for the intersection between the $3p_x$ and $3s$ states is parallel to the molecular plane, indicating that out-of-plane motions are not necessary. Therefore, the major difference between the β_{eff} values for channels I and II originates in the $3s$/ground-state coupling, and not in the $3p_x/3s$ coupling. The O–D bond dissociation observed at 352.5 nm following excitation to the $3s$ state gives rise to the same β_{eff} as observed following initial excitation to the $3p_x$ state.[13] This further confirms that the pathway from $3s$ to the ground state dictates the β_{eff} value.

No conical intersection calculations have yet been carried out for the $3p_z$ state. However, because no significant change in the H/D ratio is observed when the radical is excited to the $3s$, $3p_x$, or $3p_z$ states (see above), dissociation from the $3p_z$ state probably proceeds via multiple surface crossings. After the radical is excited to the $3p_z$ state, it first couples to the lower Rydberg states and, finally, to the ground state. The H/D ratio is therefore determined by the same final step. This interpretation is supported by Franck–Condon considerations. The Rydberg $3s$, $3p_x$, $3p_y$, and $3p_z$ states (at 3.22, 4.34, 4.89, and 5.09 eV, respectively) have planar geometries resembling the ground-state ion, and they are close in energy. Therefore, in the dissociation from the $3p_z$ state, the Franck–Condon factors are more favorable for inter-Rydberg couplings than for direct coupling to the ground state, and multiple surface crossings are expected en route to the dissociative state.

Simultaneous O–D and C–H bond rupture channels have also been predicted by Harding for the CH_2+OD reaction, which evolves via a CH_2OD intermediate.[17] Approximately 400 trajectories were propagated at an initial energy of 5.4 eV, which is close to the adiabatic energy of the $3p_z$ state (5.08 eV). In this calculation, D+CH_2O is predicted to be the major channel (57%) and H+HCOD is the second

major channel (13%). Since our experimental evidence indicates that the final dissociation step always takes place on the ground state, the trajectory calculations carried out on the ground PES provide a useful mechanistic guideline.

Figures 6 and 8 show that D and H have different $P(E_T)$ and β_{eff}. In particular, there is almost no D population at low E_T, where the maximum H population is observed. Had isomerization been important, the H and D fragments associated with this channel should have had similar $P(E_T)$. This is not observed, at least at energies below the origin band of the transition to the $3p_z$ state. Therefore, we conclude that channels I and II, and not isomerization, give rise to the H and D fragments.

B. Spectroscopic implications

As concluded above, all the low-lying excited Rydberg states and the ground state of CH_2OD are entangled by conical intersections connecting their potential energy surfaces. This intricate situation should be reflected in the excitation spectra involving these states. The predissociative nature is clearly evident in the first absorption band, which starts at $\sim 26\,000$ cm^{-1} and corresponds to the $3s(^2A')\leftarrow 1\,^2A''$ transition. This band is broad and displays no vibronic structures.[11]

Because a conical intersection between $3s$ and the ground state is expected above 2.9 eV, the nuclear dynamics no longer proceeds on the individual PESs. The strong nonadiabatic interaction renders the $3s$ state "unbound" with respect to the O–D coordinate. Along this coordinate, the excited radical is funneled through an efficient "vertical" conical intersection from the $3s$ to the ground-state surface, leading to internal conversion and rapid dissociation, which is responsible for the diffuse nature of the absorption band.[15]

In spectra involving excitations to the $3p_x$ and $3p_z$ states, vibrational structure is evident, but no rotational features can be resolved. The narrower spectra can be rationalized by considering the shape of the intersection cones between the two coupled states. The $3s$/ground-state intersection is vertical, while that between the $3p_x$ and $3s$ states is tilted.[15] Tilted cones offer ease of access, but are less efficient in promoting upper to lower-state transitions compared to the vertical ones.

C. Thermochemical values

From the maximum c.m. translational energy of the products of channel II [Fig. 3(a)], $D_0(\text{C–H}) = 3.4 \pm 0.1$ eV (79 ± 2 kcal/mol) is determined. Combining this bond dissociation energy with the known heats of formation of the H atom [$\Delta H_f^0(\text{H}) = 51.63$ kcal/mol] and CH_2OD [$\Delta H_f^0(CH_2OD) = -3.63$ kcal/mol],[4,12] the heat of formation of CHOD is estimated at $\Delta H_f^0(\text{CHOD}) = 24 \pm 2$ kcal/mol. This value is in good agreement with the one obtained by the calculation of Klippenstein, 25.49 kcal/mol.[18] The consistence between the experimental and theoretical values confirms also that the H products observed in the dissociation of CH_2OD are generated by channel II.

V. CONCLUSIONS

In this work, the photodissociation channels (I) $CH_2OD \rightarrow CH_2O + D$ and (II) $CH_2OD \rightarrow H + CHOD$ are investigated from the threshold of H atom formation to the region of the origin band of the $3p_z(^2A'')\leftarrow 1\,^2A''$ transition (30 540 and 41 000 cm^{-1}, respectively). H/D product ratios, as well as products c.m. translational energy distributions and kinetic-energy-dependent anisotropy parameters, are determined. Our main conclusions are summarized below:

(i) The D and H fragments are produced directly via channels I and II, respectively. No evidence of $CH_2OD \leftrightarrow CH_2DO$ isomerization is obtained.

(ii) Even when initial excitation accesses the $3p_x$ and $3p_z$ states, sequential couplings to the $3s$ state followed by conical intersections with the ground state access finally the dissociative ground state along the O–D and C–H coordinates, leading to channels I and II.

(iii) The branching ratio to channel II increases monotonically as the excitation energy is increased above its threshold.

(iv) The recoil anisotropy parameter corresponding to channel I from $3p_x$, $\beta_{\text{eff}} = -0.7$, is characteristic of fast dissociation. β_{eff} for channel II, however, is nearly zero, and we suggest that it may be affected by strong out-of-plane nuclear motions required for the coupling of $3s$ and the ground state, which are of A' and A'' symmetry, respectively.

(v) The experimental results are in agreement with preliminary conical intersection calculations,[15] which reveal at least one conical intersection between the $3p_x$ and $3s$ states and two between $3s$ and the ground state. In these calculations, the $g-h$ plane representation indicates that out-of-plane motions participate in the coupling between $3s$ and the ground state. A more complete understanding of the photodissociation dynamics requires additional theoretical investigations that include all the states involved in the dissociation.

(vi) The maximum translational energy for channel II is 79 ± 2 kcal/mol. From this value, the heat of formation of CHOD, $\Delta H_f^0(\text{CHOD}) = 24 \pm 2$ kcal/mol, is obtained in good agreement with the theoretical prediction.

ACKNOWLEDGMENTS

Support from the Chemical Sciences, Geosciences and Biosciences Division, Office of Basic Energy Sciences, U.S. Department of Energy, and the Donors of the Petroleum Research Fund, administered by the American Chemical Society, is gratefully acknowledged. We are indebted to Larry Harding and Stephen Klippenstein for sending us unpublished results of their calculations.

[1] J. J. Lin, J. Shu, Y. T. Lee, and X. Yang, J. Chem. Phys. **113**, 5287 (2000).
[2] J. Shu, J. J. Lin, Y. T. Lee, and X. M. Yang, J. Chem. Phys. **115**, 849 (2001).
[3] P. Pagsberg, J. Munk, A. Sillesen, C. Anastasi, and V. Simpson, Chem. Phys. Lett. **146**, 375 (1988).
[4] R. D. Johnson and J. W. Hudgens, J. Phys. Chem. **100**, 19 874 (1996).
[5] M. Ahmed, D. S. Peterka, and A. G. Suits, Phys. Chem. Chem. Phys. **2**, 861 (2000).
[6] S. Rettrup, P. Pagsberg, and C. Anastasi, Chem. Phys. **122**, 45 (1988).
[7] P. J. Bruna and F. Grein, J. Phys. Chem. A **102**, 3141 (1998); **105**, 8599 (2001).

[8] P. Pagsberg, J. Munk, C. Anastasi, and V. Simpson, Chem. Phys. Lett. **157**, 271 (1989).
[9] V. Aristov, D. Conroy, and H. Reisler, Chem. Phys. Lett. **318**, 393 (2000).
[10] C. S. Dulcey and J. W. Hudgens, J. Phys. Chem. **87**, 2296 (1983); Bull. Soc. Chim. Belg. **92**, 583 (1983); J. Chem. Phys. **84**, 5262 (1986).
[11] L. Feng, X. Huang, and H. Reisler, J. Chem. Phys. **117**, 4820 (2002).
[12] D. Conroy, V. Aristov, L. Feng, and H. Reisler, J. Phys. Chem. A **104**, 10288 (2000).
[13] L. Feng, A. V. Demyanenko, and H. Reisler, J. Chem. Phys. **118**, 9623 (2003).
[14] D. Conroy, V. Aristov, L. Feng, A. Sanov, and H. Reisler, Acc. Chem. Res. **34**, 625 (2001).
[15] B. C. Hoffman and D. R. Yarkony, J. Chem. Phys. **116**, 8300 (2002).
[16] J. A. Syage, J. Chem. Phys. **105**, 1007 (1996).
[17] L. B. Harding (private communication).
[18] S. Klippenstein (private communication).